



Contents lists available at ScienceDirect

Applied Surface Science

journal homepage: www.elsevier.com/locate/apsusc

Nanoscale morphology for high hydrophobicity of a hard sol–gel thin film

Y.L. Wu^{a,*}, Z. Chen^b, X.T. Zeng^a

^a Singapore Institute of Manufacturing Technology, 71 Nanyang Drive, Singapore 638075, Singapore

^b School of Materials Science and Engineering, Nanyang Technological University, 50 Nanyang Avenue, Singapore 639798, Singapore

ARTICLE INFO

Article history:

Received 11 February 2008

Received in revised form 1 May 2008

Accepted 1 May 2008

Available online 8 May 2008

Keywords:

Hydrophobicity
Surface morphology
Nano-structure
Sol–gel
Coating
Thin film
Contact angle

ABSTRACT

It is challenging to obtain a hydrophobic smooth coating with high optical and mechanical properties at the same time because the hydrophobic additives are soft in nature resulting in reduced hardness and durability. This paper reports a durable hydrophobic transparent coating on glass fabricated by sol–gel technology and a low volume medium pressure (LVMP) spray process. The sol–gel formula consists of a pre-linked hydrophobic nano-cluster from hydroxyl-terminated polydimethylsiloxane, titanium tetraisopropoxide and a silica-based sol–gel matrix with silica hard fillers. Polydimethylsiloxane (PDMS) is uniformly distributed throughout the coating layer providing durable hydrophobic property. Mechanical properties are achieved by the hard matrix and hard fillers with the nano-structures. Due to the surface nano-morphology, a high degree of hydrophobicity was maintained with only 10 vol.% PDMS, while the hardness and abrasion resistance of the coatings were not significantly compromised. Chemical analyses by FTIR confirmed the uniform distribution of the PDMS and surface morphology analyses by atomic force microscopy (AFM) displayed the nano-surface structures that enhanced the hydrophobicity. The special surface nanostructures can be quantified using surface Kurtosis and ratio between asperity peak height to distance between peaks. The LVMP process influences the spray droplet size resulting in different surface structures.

© 2008 Elsevier B.V. All rights reserved.

1. Introduction

Water repellent coatings providing high water repelling function and higher abrasion resistance are increasingly used on inorganic surfaces, such as glass and ceramics, for a wide range of applications including coatings for automotive windows, building surfaces, bathroom surfaces, and green house glass pannels. Hydrophobic coatings made from perfluoroalkylsilanes by sol–gel technology [1–3] have been intensively investigated, and have been used on automotive windshield and sidelights by Nippon Sheet Glass for 10 years [4]. Although three generations of coatings have been introduced, further improvements on hydrophobicity and abrasion resistance will lead to expanded market and wider application fields. Other hydrophobic reagents including long-chain organosilane compounds were reported [5–8]. Contact angles in the range of 95–115° were reported on smooth surfaces, and up to 141° on rough surfaces. It is well known that the water contact angle cannot be increased beyond 120° by a purely chemical process on smooth surface [9]. Further enhancement of contact angle is due to an increase in surface roughness. Some authors [10–12] defined superhydro-

phobic surfaces as those having water contact angle higher than 150°. Others [13–15] believed that contact angle hysteresis (the difference between the advancing and receding contact angles), rather than the static contact angle, controls the water repellency. Studies on textiles [16,17] showed that hysteresis was caused by kinetic barriers to contact line movement, both advancing and receding. On smooth surfaces, these barriers are usually from the roughness and chemical heterogeneity. It was suggested that hydrophobicity should be quantified by providing the advancing angle (θ_A) and receding angle (θ_R) and calculating the force required for a water droplet to move over the surface using the value of $\gamma_{LV}(\cos \theta_R - \cos \theta_A)$. It must be noted that increasing surface roughness decreases the transparency because of the light scattering at the rough surface. Therefore, it is always challenging to obtain high hydrophobicity on a transparent surface.

A sol–gel formulation consisting of a pre-linked hydrophobic nano-cluster from hydroxyl-terminated polydimethylsiloxane (PDMS) and titanium tetraisopropoxide (TIP), and a silica-based sol–gel matrix with silica hard fillers was developed and reported by us previously [18]. A contact angle of 133° was achieved by 50 vol.% PDMS. However, the coating hardness was reduced to 0.2 GPa from 0.85 GPa of the original sol–gel silica coating. In this paper, we further report the optimization of the chemical composition and spraying process

* Corresponding author. Tel.: +65 67938999; fax: +65 67916377.
E-mail address: ylwu@simtech.a-star.edu.sg (Y.L. Wu).

towards nanoscale structures to maximize hydrophobicity with balanced mechanical, optical and surface properties. The surfaces with different PDMS contents were characterized on their chemical groups, morphologies (surface Kurtosis (Ku), peak height and distance between peaks), stationary contact angles, advancing and receding angles. Abrasion resistance and nano-indentation hardness values were tested for optimizing the mechanical properties.

2. Experimental procedures

2.1. Materials

The coating system consists of the following components and raw materials:

- hydrophobic additive: hydroxyl-terminated PDMS, average molecular weight 550, viscosity 25 cSt,
- metal alkoxide as linker for the PDMS: titanium tetraisopropoxide,
- modifier for TIP to reduce the hydrolysis and condensation reaction rate: ethyl acetoacetate (EAcAc),
- sol-gel matrix to provide the primary strength of the coating: methyl-triethoxysilane (MTES) and tetraethyl orthosilicate (TEOS),
- silica nano-filler: 20 nm colloidal particles suspended in *iso*-butanol (pH 7),
- catalysts: acetic acid (HAc) or hydrochloric acid (HCl),
- solvents: ethanol (EtOH) and 1-propanol (PrOH).

All materials were purchased from leading chemical suppliers without further purification.

2.2. Synthesis procedures

Detailed procedures were described in our earlier publication [18]. In short, TIP/PDMS solution was prepared by mixing TIP, 1-propanol, EAcAc, PDMS and deionized water in molar ratios of TIP:PrOH:EAcAc:PDMS:H₂O = 1:6:2:2:2, which was stirred for 24 h. A stock solution of MTES and TEOS was prepared by hydrolysing these precursors in acidic water (pH 3 by adding HCl in water), followed by an addition of colloidal silica. The molar ratios of the components are: MTES:TEOS:H₂O = 1:0.016:4.4. The colloidal silica is acidified by HCl to pH 4, and added at 30 vol.% with respect to the volume of the cured solid coating. The calculation procedures for the volume percent of each component in cured solid coating was described in reference [18], and the same method was used to calculate the PDMS vol.% in this paper. The TIP/PDMS mixture was added to the MTES/TEOS stock solution in various ratios to form the final coatings with 10, 20 and 30 vol.% PDMS, in order to study the hydrophobicity and mechanical properties of the coatings.

2.3. Coating and curing processes

Coating was applied on glass substrate by a spraying process. The glass substrate was cleaned by ethanol and blown dry with N₂ gas. The air spray gun is a low volume medium pressure (LVMP) gun, which makes higher transfer efficiency and better atomization with less air consumption. This is necessary to ensure fine spray droplets and maintain a uniform transparent coating. The coated glass was dried in an oven at 80 °C for 40 min. then cured at 200 °C for 90 min. In order to fairly compare the properties of the coatings made of different chemical compositions, the coating thickness was well controlled by measuring the weight of the wet coating

during spraying. The number of spraying stocks were kept the same at first, then the weight increase of the coated sample was measured, additional spraying was performed if the weight is not enough. Since the solvent content in all the coatings were the same, the cured coatings had similar thickness between 4 and 5 μm.

2.4. Coating characterization

Coatings' hydrophobicity is measured using the VCA Optima (VCA-2500XE AST products, Inc.) contact angle machine. The image of the water drop is obtained when a pre-determined amount of water (0.5 μl) is dropped on the surface under test. The program then analyses the image of the drop and gives the contact angle value. The advancing angle is measured by dispersing additional 0.2 μl of water into the first water drop, while the receding angle is measured by withdrawing 0.2 μl of water from the drop. The difference between these two angles is the contact angle hysteresis. The force needed to move the water drop on the surface is then calculated by $F \sim \gamma_{LV}(\cos \theta_R - \cos \theta_A)$.

The chemical bonds in the coating layers were analysed by Fourier transform infrared spectroscopy (FTIR, Bio-Rad Excalibur Series). Infrared absorption spectra of the coatings in the range of 4000–600 nm wavelengths were analysed by FTIR using the attenuated total reflectance (ATR, with Ge crystal) method. An infrared radiation is passed through an infrared transmitting crystal with a high refractive index, allowing the radiation to reflect within the ATR element several times. The absorption of radiation is related to fundamental vibrations of the chemical bonds, therefore, provides information related to the presence or absence of specific functional groups in the coatings.

The surface morphology is analysed by atomic force microscopy (Veeco Scanning Prob Microscope). The 3D image of the surface topography is plotted and the surface Kurtosis and the surface area ratio (*R*, ratio between real surface area taking the height into consideration to the apparent area of flat plane) were measured. The surface Kurtosis describes the peaked-ness (peak sharpness) of the surface topography as defined by SPIP™ (Scanning Prob Image Processor, <http://www.imagemet.com/>). For Gaussian height distributions, *Ku* approaches 3.0. Smaller values indicate broader height distributions and *vice versa* for values greater than 3.0. The mean surface roughness (*R_a*) of all the samples were measured by a Tayler–Hobson Stylus Profilometer. Section analyses were performed on the topographies of the samples by AFM, and 10-point height (*R_z*) and distance between peaks (*d*) were measured. Coating's light transmittance was measured by UV-vis spectrophotometer (SHIMADZU UV-3101PC UV-vis-NIR scanning spectrophotometer).

Coating's hardness is evaluated by nano-indentations (NanoTest from Micro Materials Ltd., U.K.). The nano-indenter is a diamond Berkovich type with tip radius of 50–100 nm. The load was controlled below 0.5 mN. The resultant displacement of the indenter into the surface is monitored with a sensitive capacitive transducer and displayed in real time as a function of load. The hardness and elastic modulus are then calculated by the established equations [19] by the software. The indentation depth is controlled to be at most 10% of the coating thickness to reduce the influence from the substrate. The abrasion resistance was measured by a pin-on-disc Tribometer (ISC-200 Tribometer from Implant Sciences Corp.) using a standard Wearaser CS10 (from TABER Industries) according to ASTM D 4060. The Wearaser is in cylinder shape with a flat tip of diameter 6 mm, which is made of alumina abrasive particles embedded in resilient material. A load of 100 g was applied on the Wearaser. The test sample rotates at a speed of 500 rpm. A circular wearing track with radius about 12 mm is formed on the surface. The weight loss of the sample after

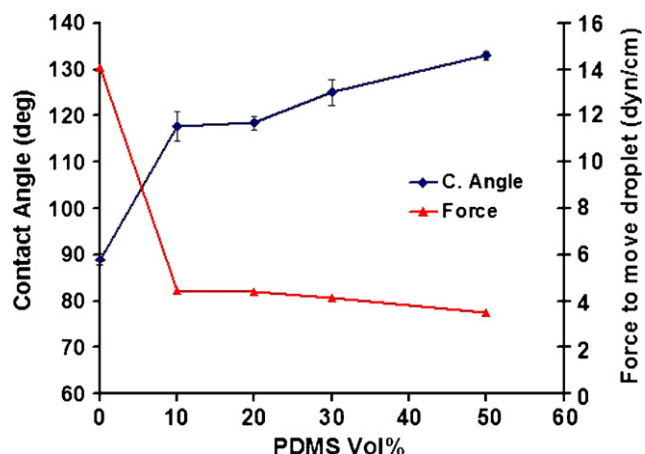


Fig. 1. Plot of water contact angle and force to move water droplet vs. PDMS content.

10,000 cycles of test is measured. Then a wear index is calculated by: wear index = weight loss (in mg)*1000/cycles. The lower the index is, the higher the abrasion resistance of the coating material. The coating layers were thick enough for this abrasion test, as we detected the layer thickness on all the samples after the abrasion tests.

3. Results and discussion

3.1. Coating's contact angle and hysteresis

The water contact angles of the coatings without PDMS and with 10, 20, 30 and 50 vol.% PDMS were measured and plotted in Fig. 1. Since the intrinsic energy of the coating material is reduced gradually by increasing PDMS content, a linear increasing trend of contact angle should be expected. However, it is seen from the graph that the contact angle remains nearly constant for coatings with 10 and 20% PDMS, and increased from 30 to 50% PDMS. The advancing and receding contact angles were also measured, and the difference between them was calculated to obtain the contact angle hysteresis. The hysteresis for coatings with 10, 20 and 30 vol.% PDMS were 3.75°, 3.70°, and 3.85°, respectively, which are quite close, while the original silica coating without PDMS showed 11.2°. This indicates that only a small tilting angle is required for the water droplet to roll off the coated surfaces, which means that the coated surfaces possess a better self-cleaning property than the original silica coated surface. The force required to move the droplet on the surface was calculated by $\gamma_{LV}(\cos \theta_R - \cos \theta_A)$, where γ_{LV} is the surface tension of water in air, which is 72 dyn/cm. The force values for 10–30% PDMS coatings were also close, which varied from 3.5 to 4.6 dyn/cm, while original silica coating needed a higher force of about 14 dyn/cm, as shown in Fig. 1 on second Y-axis. A commercial PTFE coating showed a contact angle of 97°, a hysteresis of 20° and a force of 24.5 dyn/cm. All these results indicate that, using our sol-gel synthesis route and the LVMP spray coating process, a 10-vol.% PDMS is sufficient to provide contact angle about 120° with a low hysteresis below 4°.

3.2. Chemical analysis on surfaces

Infrared absorption spectra of the 50, 30, 20 and 10% PDMS samples in wavelength range from 700 to 1400 nm are shown in Fig. 2. The major peaks in the spectra are the Si–O–Si bond

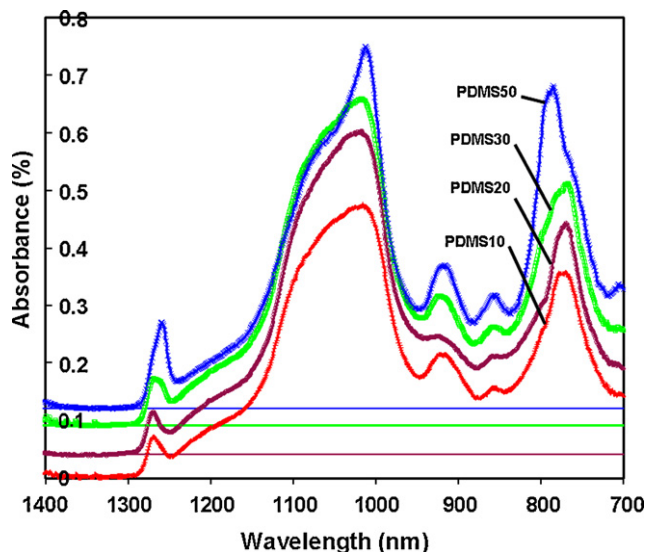


Fig. 2. FTIR absorbance spectra of coating samples containing 50, 30, 20 and 10% PDMS respectively, showing different absorption intensity confirming the uniform distribution of PDMS throughout the coating layer.

between 1000 and 1100 nm wavelength, which is from the sol-gel matrix and the silica filler. The peaks relating to PDMS content are in the ranges of 760–800 nm and 1250–1280 nm, which belong to Si–CH₃ and Si–(CH₃)₂ bonds, and in 840–860 nm, which belong to the Si–(CH₃)₂ bond. Since the absorption intensity is proportional to the presence of the specific functional groups in the coatings, we plot the intensity values of the different samples in Fig. 3 to show the relative PDMS contents in the samples. It is seen from the bar chart that the PDMS content shows increasing trend according to designed chemical compositions in the coating solution. This confirmed that the PDMS distributed uniformly throughout the coating layer rather than “float” to the outer surface. This proves that our pre-linked PDMS/TiO₂ nano-cluster is an effective route to lock the PDMS within the coating layer. The IR intensity increasing trend is similar to the increasing trend in contact angle shown in Fig. 1 except the 10% PDMS point, where the PDMS content on surface is lower, but contact angle is the same as that of 20% PDMS. To understand the reason of this behavior, we analysed the surface morphologies of the samples by AFM.

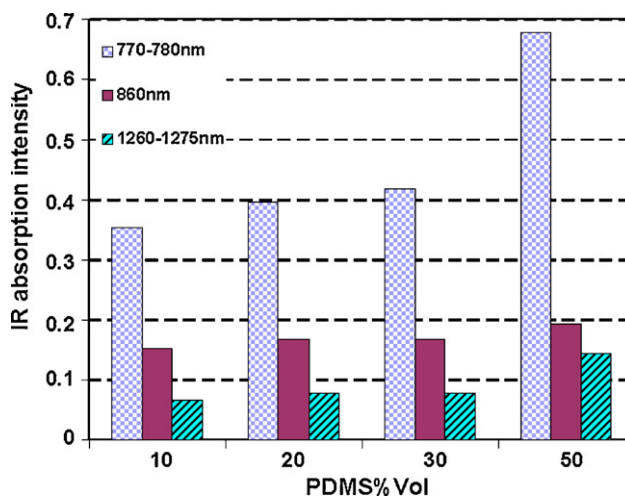


Fig. 3. FTIR absorption intensity values of peaks relating to PDMS content.

3.3. Surface topography and Kurtosis

In order to understand why the lower PDMS content (10%) coatings did not show lower contact angle and higher hysteresis than the higher PDMS content (20%) coatings, the samples without PDMS and with 10, 20 and 30% PDMS were analysed by AFM in a stepping mode. Fig. 4 shows the 3D images of the surfaces. Since all the images are in the same scale, clear differences in the peak distributions are seen. These AFM images showed that the PDMS

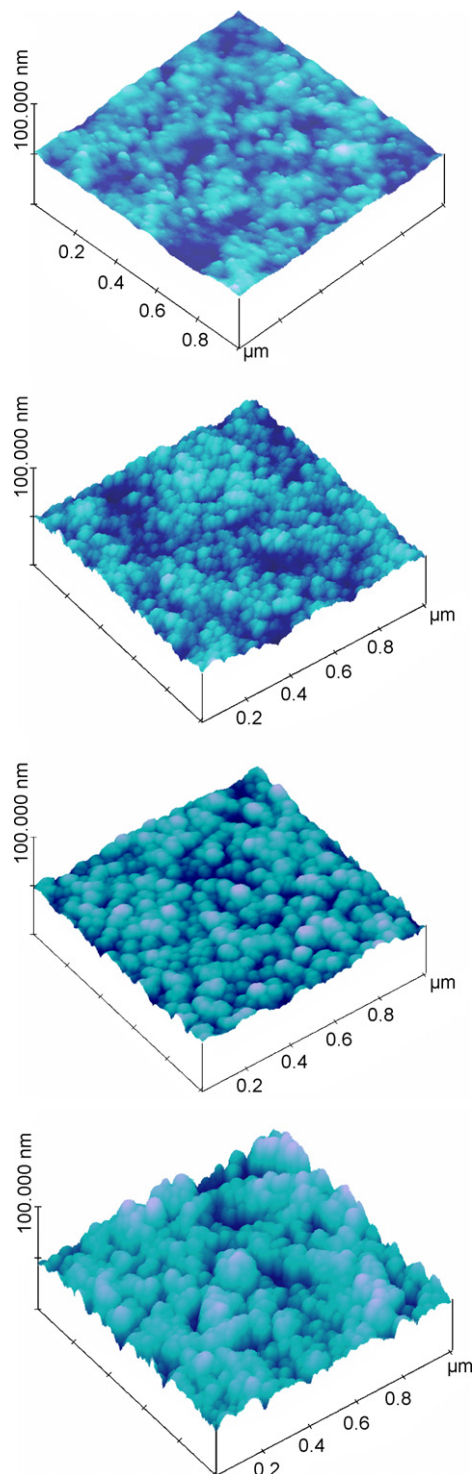


Fig. 4. AFM 3D topography images of 0 vol.% (a), 10 vol.% (b), 20 vol.% (c) and 30 vol.% (d) PDMS samples.

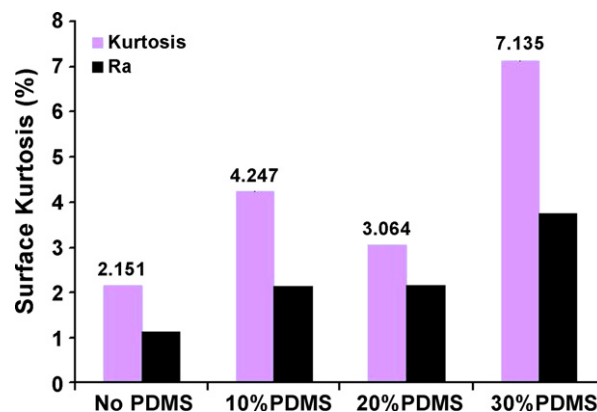


Fig. 5. Surface Kurtosis (Ku) and mean roughness (R_a) of 0, 10, 20 and 30 vol.% PDMS samples. The standard deviations of the Ku and R_a values are below 5%.

content influences not only the chemical property of the coating, but also the surface morphology due to its influence on the spraying droplets. With higher PDMS content, due to the lower intrinsic surface energy, the flow of coating solution inside the spray gun is faster under the same air pressure, resulting in bigger droplets deposited on the substrate surface. Since these droplets are dried and fixed immediately by solvent evaporation, they display broader and less sharp peaks. With less PDMS, the flow rate in the spray gun is relatively slower (due to higher friction) resulting in smaller droplets and sharper peaks. To quantify the differences in the surface morphology, we measured the surface Kurtosis (Ku), which describes the peak sharpness of the surface asperity. The commonly used mean surface roughness (R_a) values were also measured. The results are shown in Fig. 5. The R_a values show a slow increasing trend, but Ku values are not in linear trend. Ku of 10% PDMS is higher than Ku of 20% PDMS. This may be the reason why 10% PDMS showed same contact angle as the 20% PDMS although its PDMS content is lower. Ku values higher than 3 indicate a Gaussian height distributions with sharper peaks if Ku is higher. 30% PDMS displays both higher R_a and high Ku, which also showed a higher contact angle. We suggested a peak-to-valley ratio as the key parameter to correlate the surface morphology to the contact angle [8]. In that study, the surfaces were too rough to suit the AFM analysis. Therefore, only 2D profile was measured, and the peak-to-valley ratio was used as the similar parameter as Ku, and good correlation with contact angle was established. Therefore, it is confirmed again by this study that Ku is one of the useful parameter to describe the surface morphology favorable for hydrophobicity.

3.4. Theoretical models

It has been well known that hydrophobic properties are influenced by both the chemical properties and the microstructure of the solid surface. Wenzel [20] proposed the following equation for a liquid wetting a rough surface:

$$\cos(\theta_w) = R \cos(\theta_0) \quad (1)$$

where θ_w may be called the Wenzel contact angle (observed contact angle), R is the Wenzel roughness defined as the ratio of real surface area to the apparent surface area, and θ_0 the intrinsic contact angle on flat surface. To check the validity of this equation to our experimental data, we measured the R values of the 0, 10, 20 and 30 vol.% PDMS samples using AFM. After input them with the measured contact angle values into Eq. (1), we obtained the θ_0

Table 1
Calculated Wenzel model parameters

PDMS (vol.%)	Wenzel model		
	R	θ_w	θ_0
0	1.021	89.0	89.0
10	1.042	117.7	116.5
20	1.031	118.3	117.4
30	1.111	120.0	116.8

values as shown in Table 1. Since the θ_0 values are about the same for 10, 20 and 30 vol.% PDMS surfaces, while the FTIR results indicated that an increasing trend should be seen, we conclude that Wenzel equation is not suitable to describe our surfaces. According to the theoretical model of wettability versus roughness established by Pilotek and Schmidt [21], there are three regimes with increasing roughness: the smooth regime, Wenzel regime and rough regime. Yong's equation, Wenzel's equation and Cassie and Baxter's equation are suitable for the three regimes, respectively, and the hysteresis should show a small, a larger and a small value accordingly. Since our hysteresis values are quite small, it is also confirmed that our surfaces are not in the Wenzel regime. The reason is that Wenzel model assumes that water droplets fully penetrate into the surface pores and troughs. When the surface becomes rougher, it is expected that the interface under the liquid droplet assumes a composite configuration, which consists of both solid-liquid and air-liquid phases. The air trapped under the water droplets on a surface is important to the hydrophobicity of such rough surfaces.

Cassie and Baxter [22] proposed an equation (CB-equation) to describe the contact angle θ_r of a hydrophobic surface comprising an air-liquid phase and a solid-liquid phase:

$$\cos \theta_r = f_1 \cos \theta_0 - f_2 \quad (2)$$

where f_1 and f_2 are the fractions of solid-liquid and air-liquid contacting areas, respectively (i.e. $f_1 + f_2 = 1$), and θ_0 is the equilibrium contact angle on a flat surface (or called intrinsic contact angle). The equation predicts that increasing the fraction of the air-liquid area (f_2) would increase the water contact angle of the coated surface. Johnson and Dettre [23] pointed that wettability of structured surfaces should be discussed in terms of dynamic contact angle (c.a.) rather than the static. In this case, both high advancing and receding c.a. are expected and therefore a small hysteresis. Our samples showed small hysteresis (3.70–3.85°), and higher Kurtosis values than Gaussian height distribution ($Ku \sim 3$), therefore, belong to the Cassie and Baxter regime. However, it is difficult to apply this equation to real surfaces, as the determination of f_1 is complicated. Johnson and Dettre applied the CB-equation to idealized concentric grooved surfaces. Kijlstra et al. [24] extended the work of Johnson and Dettre to the wetting behavior of 1D and 2D surfaces using single and double sinusoidal models and simulations. So far, there is no direct method to measure the f_1 or f_2 of real surfaces. Ku is an indirect parameter to describe the tendency of air-trapping. But it seems not sufficient to reflect the real contact situation between a water drop on a rough surface. The distance between the peaks of the roughness profile should also be included to describe the roughness influence on contact angle with consideration of air-trapping. Veeramuneni et al. [25] studied the ion-plated PTFE (polytetrafluoroethylene) coatings and found the maximum elevation and average distance between elevations (or peaks) are significant to alter the wetting behavior of different PTFE surfaces. Fig. 6 is a schematic diagram describing the peak height (R_z is the 10-point average peak height from center line), distance between peaks (d), and the contact

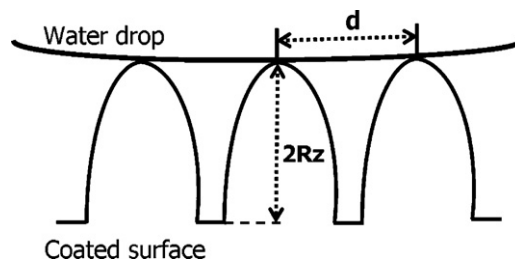


Fig. 6. Schematic diagram of contact between water drop and the rough surface showing the 10-point average peak height from center line (R_z), distance between peaks (d).

Table 2
Peak height, distance between peaks and calculated ratio between the height and the distance (f)

PDMS (vol.%)	R_z (nm)	Distance (d , nm)	Ratio (f)
0	9.82	83.8 ± 16.8	0.23
10	16.99	90.0 ± 13.7	0.38
20	17.92	132.3 ± 20.4	0.27
30	42.20	141.2 ± 18.8	0.60

condition between a water drop and the rough surface with trapped air. For more air-trapping, higher ratio between peak height to distance between peaks is beneficial. For the 0, 10, 20 and 30 vol.% PDMS samples, we took the section analyses in AFM results and measured the peak height R_z , the distance between peaks (d , average of 20 measurements) and calculated the ratio (f) between these two parameters using the following equation:

$$f = \frac{2R_z}{d} \quad (3)$$

The calculated results are listed in Table 2.

Fig. 7 shows the original profiles of sections of the samples obtained from AFM. From these profiles and the data in Table 2, we notice that the 10% PDMS sample has higher ratio than 20% PDMS sample, and 30% PDMS sample has the highest ratio. The 10% PDMS sample has higher peaks than the 0% PDMS surface but with similar distance between peaks, therefore, provides higher tendency of air-trapping. The 20% PDMS sample has similar peak height as the 10% PDMS sample, but with wider distance between peaks, which tends to allow water to sink into the trough. The 30% PDMS sample has much higher peaks with similar distance between peaks as the 20% PDMS, therefore, possesses higher tendency of air tapping. In

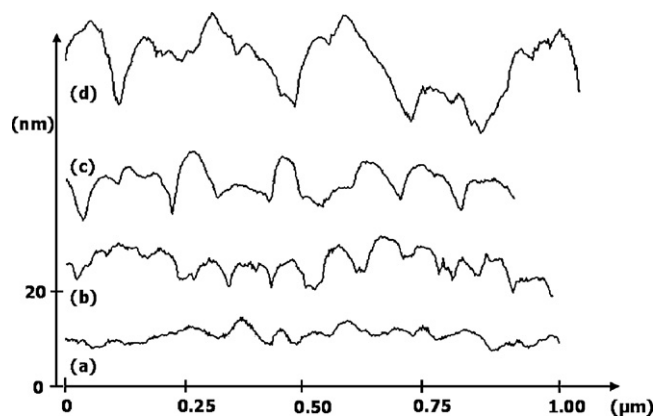


Fig. 7. Original profiles of samples from section analyses by AFM. (a) No PDMS, (b) 10% PDMS, (c) 20% PDMS and (d) 30% PDMS.

addition, the 10% PDMS surface asperity peaks present a mushroom-like shape, which further enhances air-trapping [26]. These explain why the 10% PDMS surface still shows similar contact angle as the 20% PDMS although with less PDMS. Taking a reference value of contact angle 100° of a smooth PDMS containing surface [27], we calculated the f_2 value from the CB-equation for 10% PDMS surface ($\theta_r = 118^\circ$) and obtained 35.2%, which is the air-trapped fraction of the surface area. This shows that the Cassie and Baxter's model may be also suitable for relatively smooth surfaces as long as the surface profile contains higher ratio of peak height to distance between peaks and the peaks are in mushroom-like shape, which favors air-trapping. The peak height can be as small as 6 nm as reported [27,28]. Therefore, the ratio and the surface Kurtosis value are the useful parameters to quantify the surface structure in relation to air-trapping.

From the above discussions, we can conclude that the PDMS volume content in the coating play the major role for the hydrophobicity, while the surface topography created by 10% PDMS and the LVMP spray process induced high tendency of air-trapping, therefore, increased the hydrophobicity. Since this topography contains only small peaks, the light transmittance of the coated sample is not affected. All the samples reported in this study have the same light transmittance as the glass substrate ($\geq 92\%$) measured by UV-vis spectrophotometer. This is due to the minimized light scattering by the random nano-structure with the length scale much smaller than the light wavelength [29]. Therefore, the unique nanoscale morphology formed by our process and the above analyses provide an insight on the combined effects of material surface energy and surface nanostructures on the overall hydrophobic behavior of the surface.

3.5. Coating's mechanical properties

Coating's mechanical properties are influenced by chemical composition and curing profile. Since curing profile has been optimized and reported in our previous publication [18], the effects of coating chemical compositions are presented in this paper and the preferred curing profile is adopted. Coating's mechanical properties are evaluated by nano-indentation hardness and abrasion resistance. Fig. 8 plots the nano-indentation hardness and the contact angle values in one graph in order to select an optimal PDMS content. It is seen that hardness drops almost linearly with increasing PDMS content. This is understood because PDMS is an elastomer, being soft in nature, certainly reduces the material' hardness. From the two curves in Fig. 8, it is obvious that the optimum PDMS content is 10 vol.%, which results in contact angle of 118° and hardness of 0.68 GPa. Fig. 9 shows the

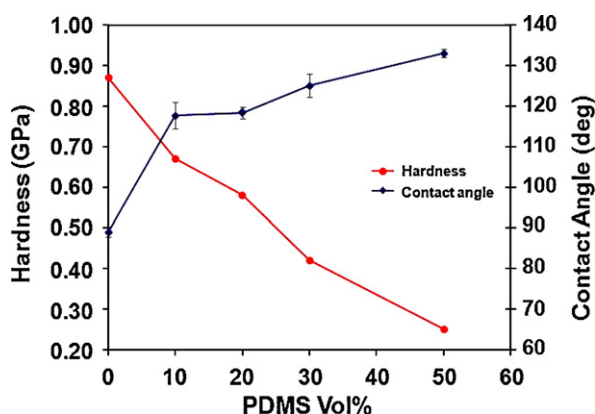


Fig. 8. Plot of nano-indentation hardness and contact angle against PDMS vol.%. The standard deviations of the nano-indentation hardness values are below 5%.

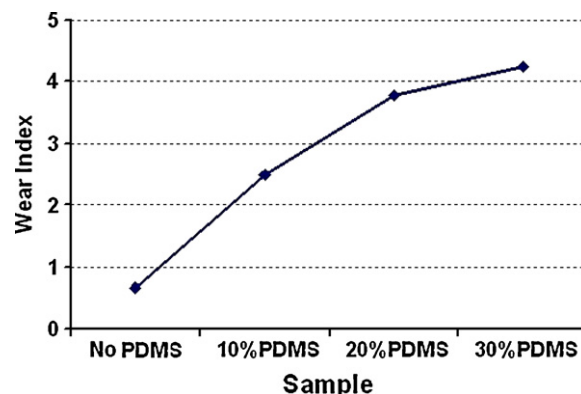


Fig. 9. Wear index of 0, 10, 20, and 30 vol.% PDMS samples tested by Weraser CS-10 on pin-on-disc machine under 100 g load for 10,000 cycles. The standard deviations are below 10%.

wear index of the 0, 10, 20 and 30 vol.% PDMS samples. As the wear index reflects the weight loss per cycle, the lower the wear index the better the wear (or abrasion) resistance. As the figure shows that 10% PDMS is better than 20% PDMS and 30% PDMS. This confirms the optimum PDMS content being 10 vol.%.

4. Conclusions

A transparent hydrophobic hard coating containing pre-linked PDMS-TiO₂ nano-cluster in silica matrix has been formulated by sol-gel route and applied to a glass substrate by a LVMP spraying process. The PDMS is uniformly distributed throughout the coating layer as proven by the FTIR analysis. The optimum PDMS content is 10 vol.%, which results in a combination of high water contact angle (118°), small contact angle hysteresis (3.75°), high nano-indentation hardness of 0.68 GPa and good abrasion resistance. The high contact angle of 10% PDMS is due to the nanoscale surface morphology that contains high peak to distance ratio, mushroom-like peaks with Kurtosis value higher than 3. This morphology is related to the LVMP spraying process which forms smaller size droplets than the higher PDMS% samples and, meantime, remains the high transparency of the coating. These results suggest that the Cassie and Baxter's model is also applicable to relatively smooth surfaces when the roughness peaks are in mushroom-like shape and the ratio of peak height to distance between peaks is high enough leading to air-trapping under the water drop on the surface.

References

- [1] H. Jeong, D. Kim, S. Lee, S. Kwon, K. Kadono, J. Colloid Interf. Sci. 235 (2001) 130.
- [2] G. Gu, Z. Zhang, H. Dang, Mater. Res. Bull. 39 (2004) 1037.
- [3] A. Nakajima, K. Abe, K. Hashimoto, T. Watanabe, Thin Solid Films 376 (2000) 140.
- [4] T. Muromachi, T. Tsujino, K. Kamitani, K. Maeda, J. Sol-Gel Sci. Technol. 40 (2006) 267.
- [5] A.V. Rao, R.R. Kalesh, J. Sol-Gel Sci. Technol. 30 (2004) 14.
- [6] W.A. Daoud, J.H. Xin, X. Tao, Appl. Surf. Sci. 252 (2006) 5368.
- [7] S. Smitha, P. Shajesh, P. Mukundan, T.D.R. Nair, K.G.K. Warriar, Colloids Surf. B: Biointerf. 55 (2007) 38.
- [8] L.Y.L. Wu, A.M. Soutar, X.T. Zeng, Surf. Coat. Technol. 198 (1–3) (2005) 420.
- [9] S.D. Bhagat, Y.H. Kim, Y.S. Ahn, Appl. Surf. Sci. 253 (2006) 2217.
- [10] E. Hosono, S. Fujihara, I. Honma, H. Zhou, J. Am. Chem. Soc. 127 (2005) 13458.
- [11] J.T. Han, X. Xu, K. Cho, Langmuir 21 (2005) 6662.
- [12] G. Zhang, D. Wang, Z.Z. Gu, H. Mohwald, Langmuir 21 (2005) 9143.
- [13] L. Gao, T.J. McCarthy, Langmuir 22 (2006) 5998.
- [14] W. Chen, A.Y. Fadeev, M.C. Hsieh, D. öner, J.P. Youngblood, T.J. McCarthy, Langmuir 15 (1999) 3395.
- [15] D. öner, T.J. McCarthy, Langmuir 16 (2000) 7777.
- [16] J.P. Youngblood, T.J. McCarthy, Macromolecules 32 (1999) 6800.
- [17] L. Gao, T.J. McCarthy, Langmuir 22 (2006) 2966.
- [18] L.Y.L. Wu, G.H. Tan, X.T. Zeng, T.H. Li, Z. Chen, J. Sol-Gel Sci. Technol. 38 (2006) 85.

- [19] W.C. Oliver, G.M. Pharr, *J. Mater. Res.* 19 (2004) 3.
- [20] R.N. Wenzel, *J. Phys. Colloid Chem.* 53 (1949) 1466.
- [21] S. Pilotek, H.K. Schmidt, *J. Sol–Gel Sci. Technol.* 26 (2003) 789.
- [22] A. Cassie, S. Baxter, *Trans. Faraday Soc.* 40 (1944) 546.
- [23] R.E. Johnson, R.H. Dettre, Contact angle, wettability and adhesion, advances in chemistry series, *Am. Chem. Soc.* 43 (1964) 112.
- [24] J. Kijlstra, K. Reihls, A. Klamt, *Colloids Surf.* 206 (2002) 521.
- [25] S. Veeramasuneni, J. Drelich, J.D. Miller, G. Yamauchi, *Prog. Org. Coat.* 31 (1997) 265.
- [26] J. Bico, U. Thiele, D. Quéré, *Colloids Surf. A: Physicochem. Eng. Asp.* 206 (2002) 41.
- [27] K. Kamitani, T. Teranishi, *J. Sol–Gel Sci. Technol.* 26 (2003) 823.
- [28] B. Wu, G. Mao, K.Y. Simon Ng, *Colloids Surf. A: Physicochem. Eng. Asp.* 162 (2000) 203.
- [29] Y.C. Chang, G.H. Mei, T.W. Chang, T.J. Wang, D.Z. Lin, C.K. Lee, *Nanotechnology* 18 (2007) 285303.